Thermodynamic Modeling of Refractory – Mold Slag – Steel Interactions Concerning Slag Crawling

E. Moosavi-Khoonsari, E. Zinngrebe, S. van der Laan, R. Kalter, F. Mensonides, Tata Steel, the Netherlands

Elmira Moosavi-Khoonsari, Tata steel, IJmuiden, Building 3J-22, Rooswijkweg 211 1951 MD Velsen-Noord NL, +31 2514 99551, elmira.moosavi-khoonsari@tatasteeleurope.com

Summary
Mold slag crawling down the outside of the submerged entry nozzle (SEN) may occur during continuous casting of steel affecting the SEN port geometry and steel flow patterns in the mold, and leading to defect formation in the final product due to slag accumulations shearing off from the SEN body. There are two possible mechanisms contributing to slag crawling, (a) refractory wetting together with chemical reactions at the refractory – mold slag – steel interface, and (b) liquid steel flow induced drag forces, displacing slag down the SEN. In this work, we applied thermodynamic modeling to study the extent of chemical reactions at the refractory – slag – steel interface using FactSage 7.2 thermochemical software. The modeling was validated by industrial and experimental observations of slag crawling. A finite number of reaction zones was identified at the interface, and it was assumed chemical reactions reach equilibrium in the designated effective reaction zone volumes. The refractory – slag carbothermic reaction, slag – steel exchange reaction, gas back-infiltration into the refractory body, and deposit formation on the SEN, observed in steel continuous casting, were investigated in detail. Thermodynamic insight into interfacial chemical reactions form the basis for successful development of the process kinetic model.

Key Words
Continuous casting, Submerged entry nozzle, Slag crawling, Chemical reactions, Thermodynamic modeling

Introduction
Slag crawling is mold slag movement from the liquid pool down the steel – submerged entry nozzle (SEN) interface beyond the slag lining further to the SEN port or even inside followed by back-circulation and draining off the modified mold slag into the original pool. The two possible mechanisms contributing to slag crawling are refractory wetting together with chemical reactions at the SEN – mold slag – steel interface, and liquid steel flow induced drag forces displacing the slag down the SEN [1]. Whether or not slag crawling occurs is likely to depend on choice and combination of mold flux, steel and SEN type however, it has been often left unexplored or ignored. Slag crawling can be among entrainment mechanisms of mold slag in the steel pool during continuous casting which could bring in risks for castability and casting stability. Wear and hole development in the SEN by crawling slag may eventually lead to its disintegration, and the change in the SEN morphology disturbs the flow regime in the mold. The mold slag composition and thermophysical properties can change due to mixing back of the contaminated mold slag into the original slag pool.
The classical view of attack on the SEN was described as dissolution of refractory oxide components in the mold slag and graphite in steel [2-4]. Harmuth and Xia [5] modeled the SEN – slag – steel interaction at zirconia anticorrosion band considering only one reaction zone, where the three reactive volumes reached equilibrium. However, a strong SEN attack associated with undercut development at the zirconia/carbon – alumina/carbon interface, observed in plant operation, suggests that the interaction in and around the SEN is more complex than it has been often assumed.
The aim for refractory life-time extension cannot be achieved unless the interfacial reactions at the SEN – mold slag – steel are well understood and can serve to guide the materials and process optimization / design. Thermochemical modeling gives insight into complex chemical reactions at the interface and mold slag entrainment mechanism and thermophysical property alteration.
In this work, the SEN – mold slag – steel interactions were modeled from equilibrium thermodynamic point of view mainly based on laboratory scale cup experiments. The observations of the cup-experiments have been presented in our companion paper [6].

Thermodynamic modeling
Figure 1 illustrates the sketch of the vertical cross-section of the refractory cup containing steel and mold slag from the experiment along with the reaction zones considered in this study. The steel and slag were both entirely molten, and the mold slag crept around the steel at the refractory interface. The gas bubble together with steel show a typical elephant foot wear appearance. Deep concave bites out of the refractory sidewalls and severe refractory destruction are observed in the experiments.
As shown in Figure 1, in addition to the refractory

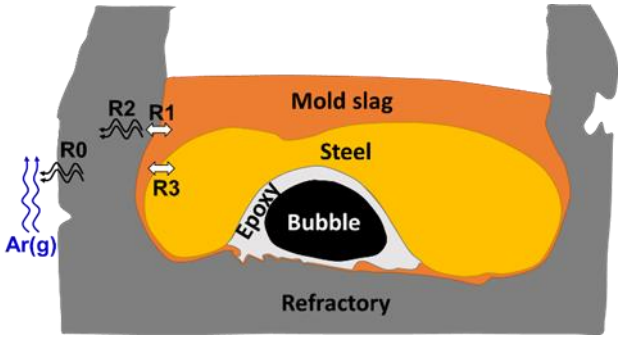

Figure 1. Schematic of the vertical cross-section of the refractory cup containing steel and mold slag, and representation of the reaction zones in the present equilibrium model

self-reaction (R0), three main contact reaction zones, refractory – mold slag (R1), refractory – gas (R2) and mold slag – steel (R3), were identified. The reaction zones were calculated one by one in the order of reaction number, and outcomes of the previous reactions were entered as inputs of next calculations in the simulation. The flow of calculations is illustrated in Figure 2. According to the 1 min cup experiment [6], the assimilation rate of refractory components

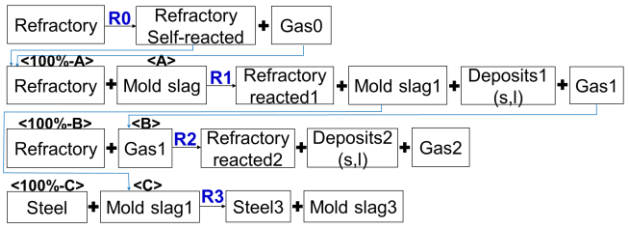

Figure 2. Flow of the calculations in the current model

including Al_2O_3 by the mold slag is faster than the mold slag – steel exchange reaction, $3(SiO_2) + 4[Al] = 2(Al_2O_3) + 3[Si]$, where ( ) and [ ] denote in the mold slag and steel, respectively. Electron Probe Micro Analysis (EPMA) showed that while the mold slag picked up a considerable amount of Al_2O_3, 21.9 wt% for the 1 min experiment (the original Al_2O_3 content of mold slag was ~ 3 wt%), steel had maintained its original Al content (0.7 wt%).

The equilibrium calculations were carried out using FactSage 7.2 thermochemical software [7]. Thermodynamic descriptions of molten steel and those of oxides including both mold slag and refractory were taken from the FSstel and CON2 databases, respectively (CON2 is a proprietary database of the "Steelmaking Consortium" developed at High Temperature Thermochemistry Laboratory, which was previously at McGill University, Canada, and is now at Seoul National University, South Korea). Thermodynamic properties of pure substances and gaseous species were adopted from the FactSage FactPS database. The Reactions R1, R2 and R3 were calculated at 1570 °C under 1 bar total pressure corresponding to the condition of the cup experiments.

The compositions of refractory cup, mold slag normalized without carbon, and steel used for the calculations are given in Table 1. The steel contained high amounts of Al, 0.7 wt%. The starting composition of the mold slag was analyzed for its elemental constituents using X-Ray Fluorescence (XRF) at Tata Steel ANAlytical laboratory, and its composition is reported in the form of oxides and pure F. However, F exists as fluorides, and to overcome overestimation of the mold slag oxygen content, pure F was converted to NaF and then CaF_2 (see Table 1).

Table 1. Chemical compositions of refractory, mold slag and steel used in the calculations (in wt%)

Refractory
Al_2O_3 (65.93), C (22.71), SiO_2 (5.23), ZrO_2 (5.13), Na_2O (0.90), SiC (0.10)
Mold slag (normalized as C free)
CaO (36.52), SiO_2 (36.09), Na_2O (12.93), F (9.57), Al_2O_3 (3.15), MgO (0.76), FeO (0.54), K_2O (0.43)
**SiO_2 (37.61), CaO (35.53), NaF (18.26), CaF_2 (3.52), Al_2O_3 (3.28), MgO (0.79), FeO (0.56), K_2O (0.45)*
Steel
Mn (2.08), Al (0.71), Cr (0.20), C (0.15), Si (0.11), Ti (0.02), B (0.02), P (0.01), S (0.005)

**The mold slag composition recalculated in the form of NaF and CaF_2 constituents.*

Refractory self-reaction (R0)

Figure 3 illustrates that the refractory undergoes self-reaction at 1570 °C. Al_2O_3, C, slag, ZrO_2 and mullite are the stable phases under 1 bar total pressure while ZrC forms at reduced pressure. Indeed, within the refractory body, ZrC particles were found, as seen in Figure 4, which cannot be stable under 1 bar total CO pressure. The ZrC cubes are readily distinguishable from the ZrO_2 blobs in the cross-section microstructure. At pressures below ~ 0.5 bar, Al_2O_3, C, gas phase, ZrC and SiC are stable components of the refractory.

In addition to the experimental observation, the ZrC cubes and SiC particles were found in post-mortem SEN samples from plant confirming the under pressure (P_{Total} < 1 bar) effect within the SEN body (the microstructure image is not presented here). Fluid dynamics induced underpressure, transmitted into the SEN, in combination with chemical effects (e.g. production/consumption of a gas in a confined space like porosity) makes pressure a real variable in the refractory.

As shown in Figure 3, the self-reacted refractory experiences also partial melting, consistent with the measured melt composition within the heated refractory (mainly 50 SiO_2, 35 Al_2O_3 and 11 wt% Na_2O in comparison to the experimentally measured values of 49±5, 35±4 and 10±1 wt%, respectively).

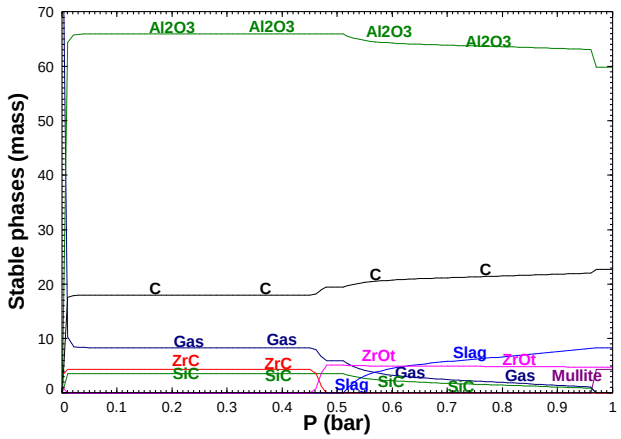

Figure 3. Refractory self-reaction (R0) calculated at 1570 °C under different total pressures

Refractory – mold slag carbothermic reaction (R1)

The equilibrium products of the refractory – mold slag interaction and their compositions are depicted in Figure 5. The figures may be read as illustrating the reaction products and their compositions across the reaction interface from the refractory bulk interface at the left of the figures to the mold slag bulk interface at the far right side of the x-axis. It is seen in Figure 5 that based on the proportions of reacted mass of refractory and mold slag, the nature of reaction products and their chemistries change. As mentioned before, the refractory bulk composition consists of Al_2O_3, C, liquid slag (mainly SiO_2, Al_2O_3 and Na_2O), mullite and tetragonal ZrO_2 at 1570 °C under 1 bar total pressure. It is seen in Figure 5(a), the mold slag can dissolve a significant amount of refractory before saturation with Al_2O_3, more than two times of its original weight. The modified mold slag from R1 is called 'mold slag1'. In addition to a small amount of gas phase 'Gas1', there are other phases like SiC and liquid Fe solution stable at the interface.
Figure 6 depicts the crystallization path of the experimental mold slag, calculated using FactSage Scheil – Gulliver Cooling mode [8] which further confirms that the experimental mold slag with the modified composition from Al_2O_3 assimilation was still above its liquidus (fully molten) at 1570 °C. That is, the mold slag was undersaturated with Al_2O_3. According to the calculations, there is about 50 °C super liquidus, and crystallization of the modified mold slag begins only upon cooling with small amounts of ZrO_2 (~ 2 wt%) at 1530 °C followed by crystallization of 3 wt% 'CM_2A_8' $CaMg_2Al_{16}O_{27}$ and 11 wt% '$C_2M_2A_{14}$' $Ca_2Mg_2Al_{28}O_{46}$ at 1350 and 1320 °C, respectively. However, the estimated break temperature corresponding to about 30 vol% solid in the mold slag is 1130 °C. Hence, the modified mold slag remains fluid, easily crawls around steel and wets it unless a process of assimilation – fractional crystallization leads to a mold slag composition that is mostly solid at 1570 °C and does not wet the SEN anymore. This is highly controlled by the phase constituents of the refractory.

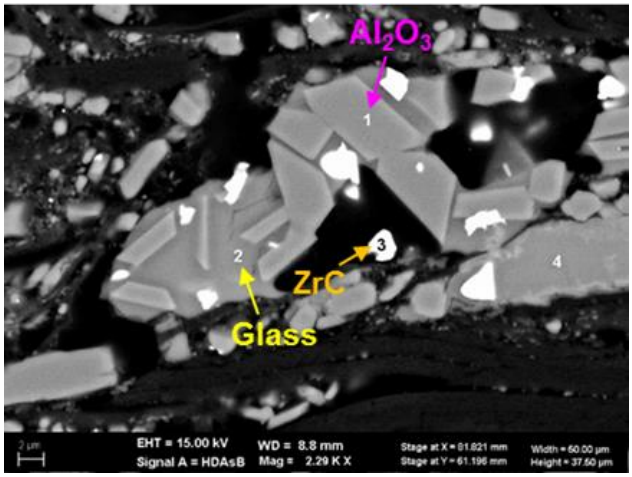

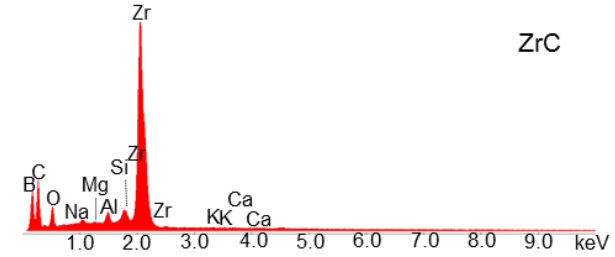

(a)

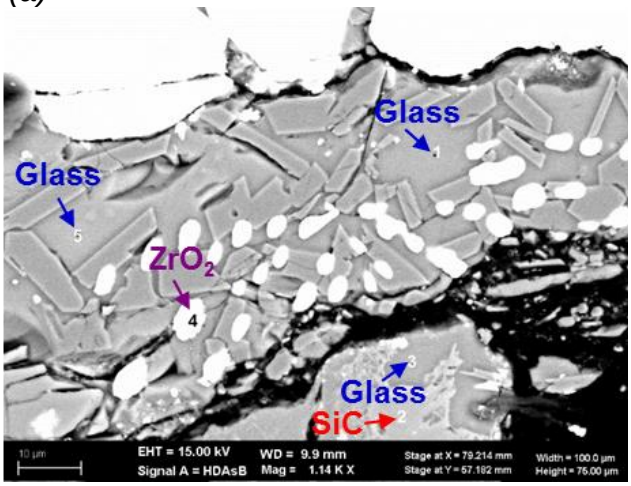

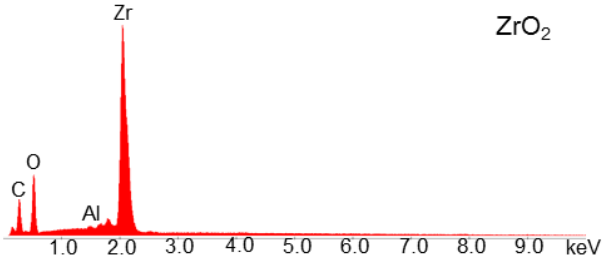

(b)

Figure 4. Microstructure of refractory cross-section, BSE images with correspondent EDS analysis; (a) ZrC + Al_2O_3 + glass and (b) ZrO_2 + Al_2O_3 + glass (glass is the quenched liquid slag)

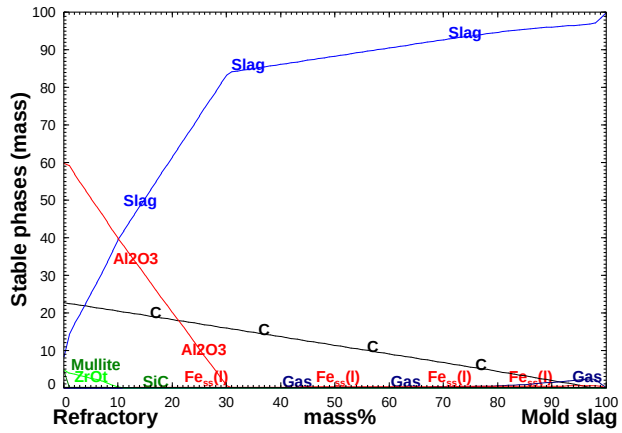
Stable phases (mass)
Slag
Slag
Slag
Al2O3
Al2O3
C
C
C
C
Mullite
ZrOt
SiC
Fe_ss (l)
Gas
Fe_ss (l)
Gas
Fe_ss (l)
Fe_ss (l)
Gas
Refractory
mass%
Mold slag

(a)

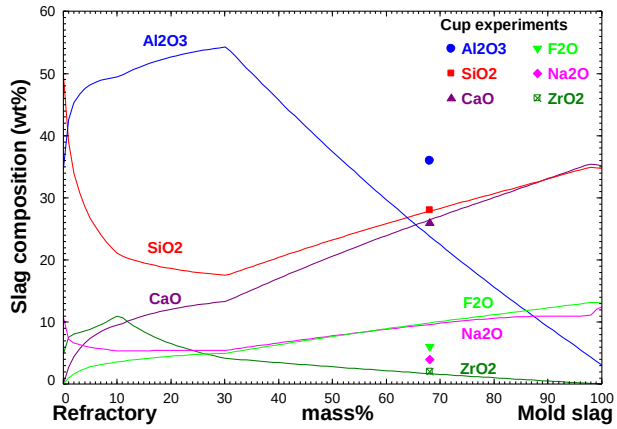
Slag composition (wt%)
Cup experiments
Al2O3
F2O
SiO2
Na2O
CaO
ZrO2
Al2O3
SiO2
CaO
F2O
Na2O
ZrO2
Refractory
mass%
Mold slag

(b)

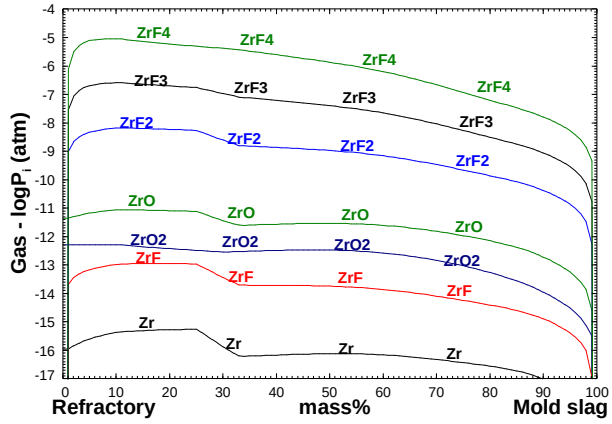
Gas - logP_i (atm)
ZrF4
ZrF3
ZrF2
ZrO
ZrO2
ZrF
Zr
Refractory
mass%
Mold slag

(c)

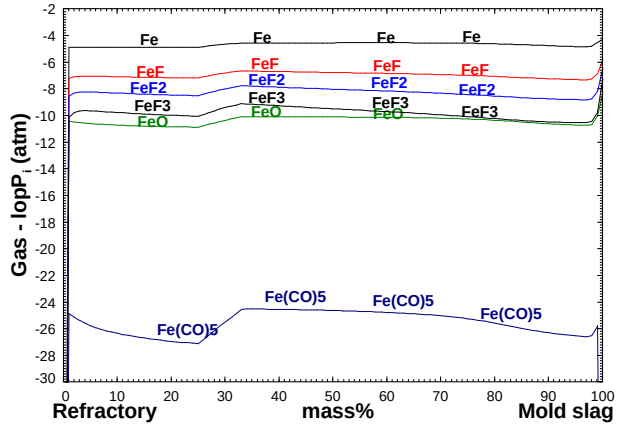
Gas - logP_i (atm)
Fe
FeF
FeF2
FeF3
FeO
Fe(CO)5
Fe(CO)5
Refractory
mass%
Mold slag

(d)

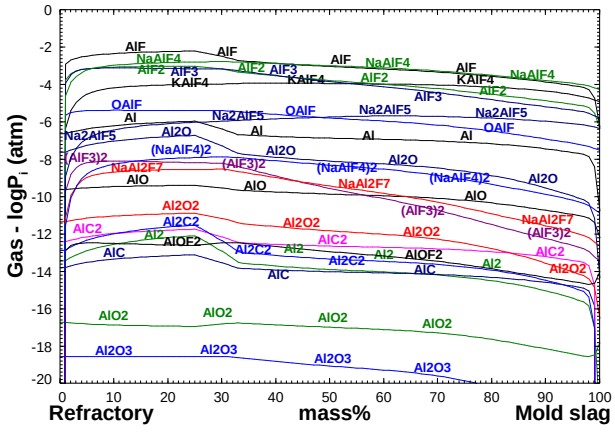
Gas - logP_i (atm)
AlF
NaAlF4
AlF2
AlF3
KAlF4
OAlF
Al
Na2AlF5
Al2O
(NaAlF4)2
(AlF3)2
NaAl2F7
AlO
Al2O2
Al2C2
AlC2
Al2
AlOF2
AlC
AlO2
Al2O3
Refractory
mass%
Mold slag

(e)

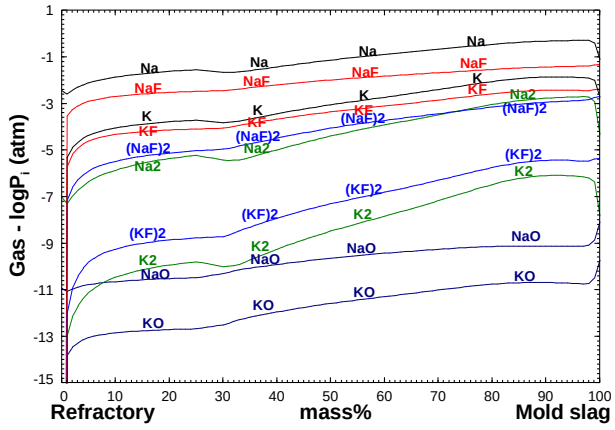
Gas - logP_i (atm)
Na
NaF
K
KF
(NaF)2
Na2
(NaF)2
(KF)2
K2
NaO
KO
Refractory
mass%
Mold slag

(f)

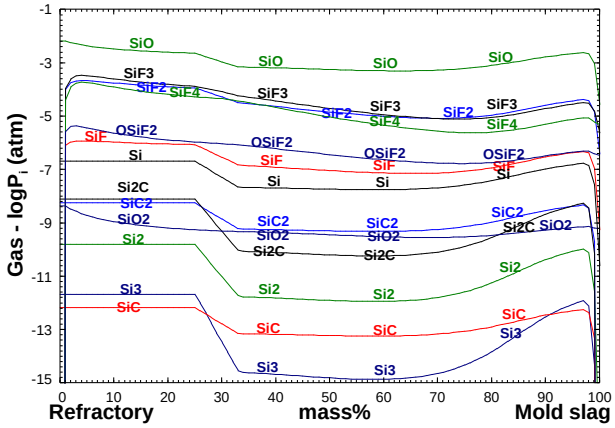
Gas - logP_i (atm)
SiO
SiF3
SiF2
SiF4
SiF
OSiF2
Si
Si2C
SiC2
SiO2
Si2
Si3
SiC
Refractory
mass%
Mold slag

(g)

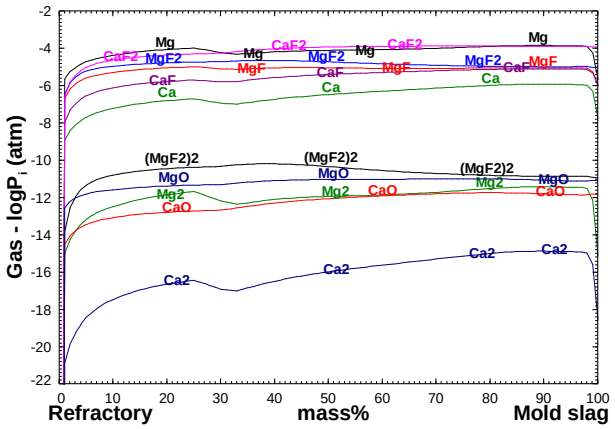
Gas - logP_i (atm)
Mg
CaF2
MgF2
MgF
CaF
Ca
(MgF2)2
MgO
Mg2
CaO
Ca2
Refractory
mass%
Mold slag

(h)

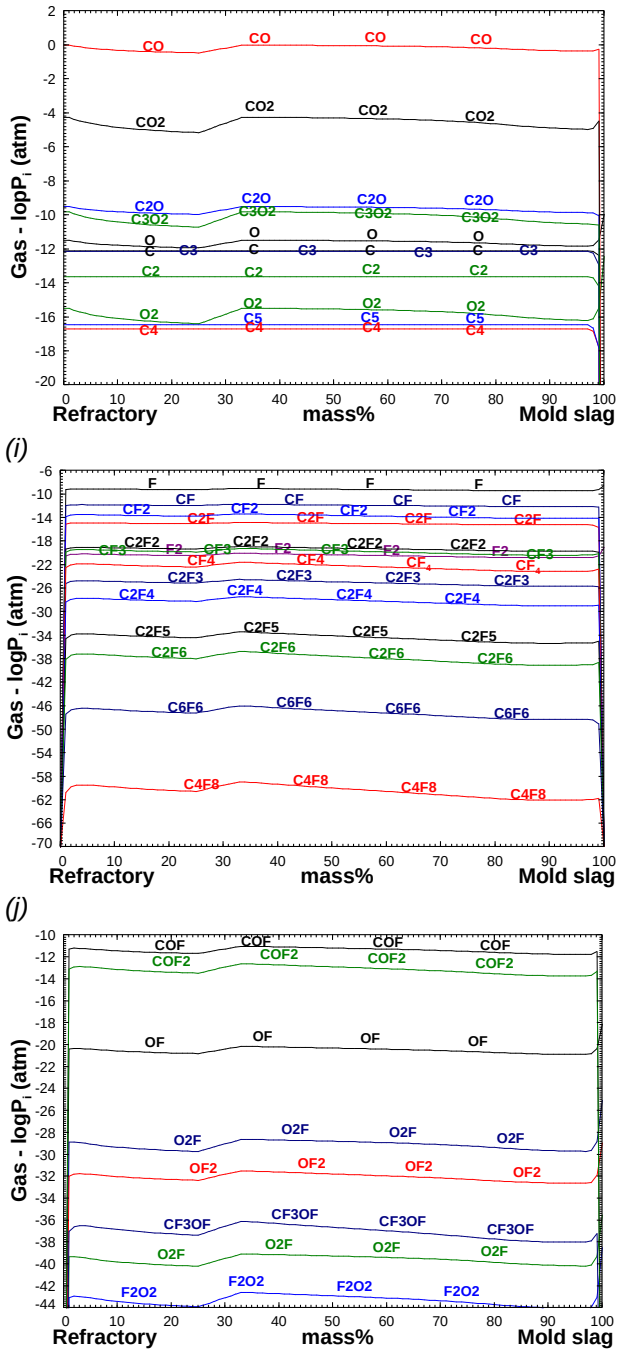

Figure 5. Reaction between the mold slag and refractory (R1) calculated at 1570 °C under 1 bar total pressure, (a) the reaction products, (b) the 'slag1' composition (symbols represent the experimental mold slag composition), and (c – k) the 'Gas1' species

In the cup experiments, the quenched mold slag consisted of ZrO_2 and plate-like metastable Al_2O_3 crystals within a glass matrix as shown in Figure 7. The formation of Ca-aluminates (CM_2A_8 and $C_2M_2A_{14}$) predicted by FactSage could be kinetically hindered, pertinent to their complex crystal structures consisting of stacked layers of spinel blocks, metastable Al_2O_3 forming instead [9].
The 'mold slag1' composition is shown in Figure 5(b). The main components of the original unreacted mold

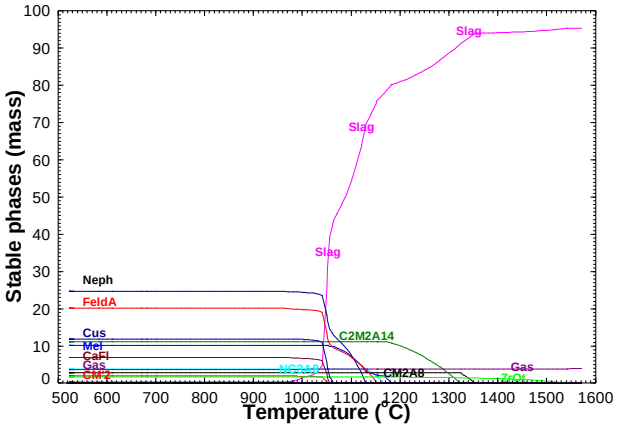

Figure 6. Fractional crystallization of the experimental mold slag after reaction with the refractory and steel. There is less than 1 wt% of other phases such as clinopyroxene, wollastonite and ZrO_2

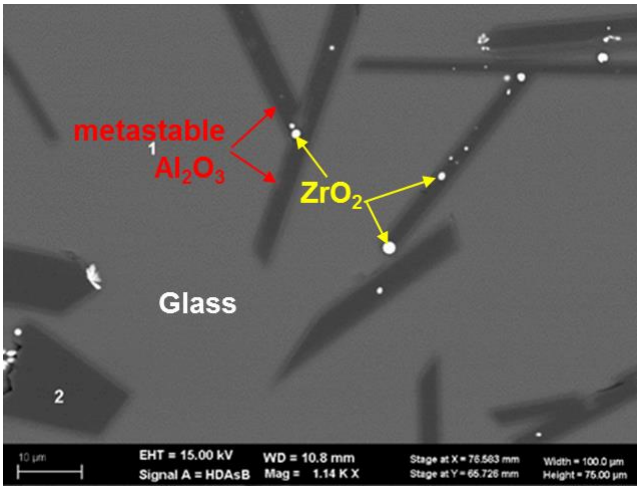

Figure 7. Crystallization of ZrO_2 and metastable Al_2O_3 within the glass matrix upon cooling of experimentally modified mold slag

slag are CaO, SiO_2 and fluorides. However, the mold slag composition changes significantly from low Al_2O_3 content (~3 wt%) to very high Al_2O_3 content due to reaction with the refractory. According to mass balance from the 10 min cup experiment, the reacted mold slag / refractory mass ratio is about 7.8/3.6 (at 68 wt% mold slag in Figure 5). This was constructed based on the amount of ZrO_2 picked up by the mold slag assuming the reaction rate of all refractory components was the same as that of ZrO_2 (the refractory is the only source of ZrO_2). The experimental mold slag composition was plotted as symbols against the calculations in Figure 5(b). As seen, the predicted Al_2O_3 content of modified mold slag is 12 wt% lower than the experimentally measured value 36 wt% from the 10 min experiment. This can be related to different assimilation rate of Al_2O_3 grains in the mold slag in comparison to that of other constituents despite the first assumption. Moreover, the mold slag composition is influenced by reaction with steel, discussed in R3, and volatilization, not considered in R1. The experimentally measured Na_2O and F

contents of mold slag are lower than the calculated ones which can be pertinent to the loss of high vapor pressure components to the gas phase.
The 'Gas 1' composition is depicted in Figure 5(c-k) where in addition to CO, other species also form. CO(g) is the dominant species in agreement with the refractory extensive decarburization and the gas bubble formation between the elephant feet at the cup bottom. The gaseous species were categorized into different groups based on the major element carrying as seen in Figures 5(c-k). The dominant species in each category are AlF, AlF_3 and AlF_4 (Al species); CaF_2 and CaF (Ca species), Fe (Fe species); K and KF (K species); Mg, MgF_2 and MgF (Mg species); Na, NaF and $(NaF)_2$ (Na species); SiO, SiF_3, SiF_2 and SiF_4 (Si species); ZrF_4 (Zr species); CO and CO_2 (C species); and $NaAlF_4$ and $KAlF_4$. After CO, the most abundant gaseous species are Na, NaF, K, $NaAlF_4$, KF and SiO.

Refractory – 'Gas1' reaction (R2)

In addition to its main components Al_2O_3, ZrO_2 and C, the SEN consists of various glassy phases, zirconia-mullite (ZM) aggregate glass and zirconia-C (ZC) additive glass, which compositions are depicted as star and diamond in Figure 8, respectively (the glass composition was measured in unused SEN samples). The Al_2O_3-C band contains ZM aggregates, an alkaline Ca-free albite-like glass. The glass composition slightly varies, and the stars on the graph cover its compositional range. The expected compositional change of glass via reduction by internal refractory C is shown by the black dashed vector in Figure 8. Moreover, the SEN inside is covered with a two-layer glaze, an alkaline layer and a very silicic glass layer, to prevent the premature C burn-off to open atmosphere during preheating. The original mold slag composition (35 SiO_2, 3 Al_2O_3, 35 CaO and 12 Na_2O in wt%) is marked as filled square in the figure. The mold slag can be reduced by (a) steel according to reaction $3(SiO_2) + 4[Al] = 2(Al_2O_3) + 3[Si]$ (the slag gains 2 moles of Al_2O_3 at the expense of 3 moles of SiO_2) and (b) carbon according to reaction $(SiO_2) + C = CO(g) + SiO(g)$ (the mold slag loses SiO_2 to the vapor phase in the form of SiO(g)). The two reduction vectors of mold slag are shown in Figure 8 as green and red dashed lines, respectively.
However, little droplets of molten slag (glass at low temperature) were found within the body of SEN post-mortem samples after casting having different compositions in comparison to ZM, ZC and glaze within the unused SEN and mold slag. The question was then raised about the horizontal element mobility across the porous refractory layers, possible transport media and driving force. Elements could be transported to the refractory bulk via back-infiltration of either the mold slag or gas phase under an existing pressure or chemical gradient across the SEN.
Thermodynamic modeling aids in understanding the mechanism governing the formation of molten slag

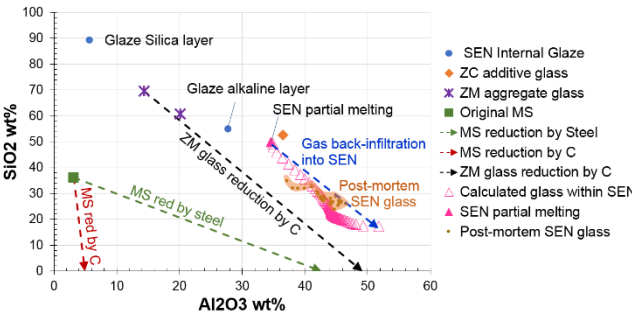

(a)

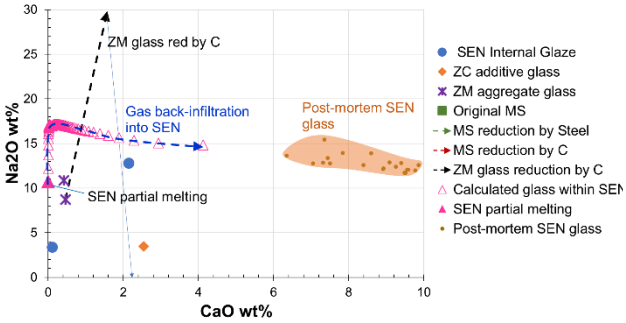

(b)

Figure 8. SEN glass and mold slag compositions (a) SiO_2 vs. Al_2O_3 and (b) Na_2O vs CaO, along with the calculated glass composition from R2 ('Gas 1' back-infiltration reaction in the SEN body) and glass composition within post-mortem samples. ZC, ZM and MS stands for zirconia-carbon, zirconia-mullite and mold slag, respectively (for more explanation see the text)

(glass at low temperature) across the refractory body, which is detrimental to SEN integrity and can contribute to undercut formation in operation. As shown in Figures 5(c-k), since 'Gas1' contains CO, Na, Al, Ca, K, Mg, Si, Fe and Zr bearing species, the occurrence of phases in addition to those found in the self-reacted refractory, and substantial removal of refractory components such as Zr can be explained by gas back-infiltration phenomenon. The refractory – 'Gas1' reaction (R2) was, therefore, calculated to simulate gas back-infiltration reaction in the refractory bulk and subsequent recondensation. If 'Gas1' the product of mold slag – refractory carbothermic reaction back-infiltrates through the refractory porous structure under strong CO undersaturation, it reacts with the solid and liquid components of the refractory. The reaction products (the liquid 'slag2' and $NaAl_9O_{14}$) and slag composition are illustrated in Figure 9. In the real process, CO undersaturation can occur due to steel momentum in the mold.
As shown in Figure 9(b), the 'slag2' dissolves Al, Na, Zr and F gaseous species, and decrease in slag SiO_2 content is the dilution effect. The 'slag2' pool composition changes in reaction with the gas phase so that the original siliceous slag in the refractory bulk enriches in Al_2O_3 quickly. At the expense of the refractory Al_2O_3 grains, $NaAl_9O_{14}$ deposits at the interface, which content decreases after the complete consumption of Al_2O_3 (see Figure 9(a)). As said

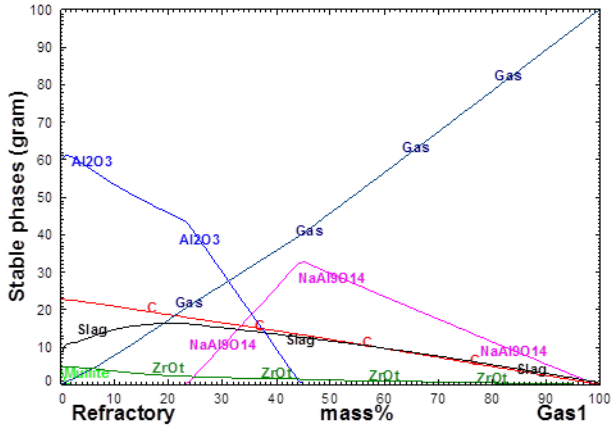

(a)

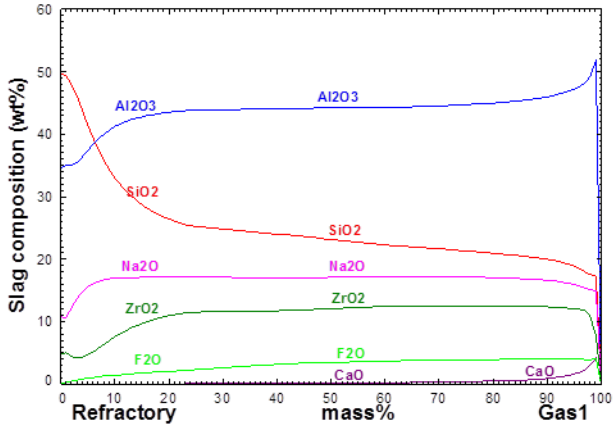

(b)

Figure 9. Reaction between the refractory and 'Gas1' (R2) calculated at 1570 °C under 1 bar total pressure, (a) the reaction products, and (b) the 'slag2' composition

before, the SEN deposits are harmful to the SEN integrity and bring in castability risk.

The liquid slag composition (glass at low temperature) calculated to form within the SEN body (marked as triangles in Figure 8) from the refractory – 'Gas 1' carbothermic reaction (R2) can be clearly distinguished from the original mold slag and SEN glass compositions. Observations over the SEN post-mortem samples (based on a well-controlled complete data set) revealed the occurrence of a glassy phase with compositions illustrated in Figure 8. The agreement between the predicted and observed glass compositions is good for Al_2O_3, SiO_2 and Na_2O however, the post-mortem glass contained higher amounts of CaO which could be the influence of Ca treated steel. Steel adds CaS and Ca aluminates to the inner side of the SEN, and Ca spreads into the refractory.

Mold slag – steel reaction (R3)

As mentioned before, the cup experiments revealed that the mold slag – refractory reaction rate is faster than that of mold slag – steel reaction, and at the time the mold slag reacted with steel, it had already reacted with the refractory and its composition had changed to 'mold slag1'. The reaction products of steel and 'mold slag1' (see R1 at 67 wt% mold slag) and their compositions are shown in Figure 10. The mold slag picks up Al_2O_3 and steel picks up Si according to the exchange reaction $4[Al] + 3(SiO_2) = 2(Al_2O_3) + 3[Si]$, where [ ] and ( ) denote in steel and

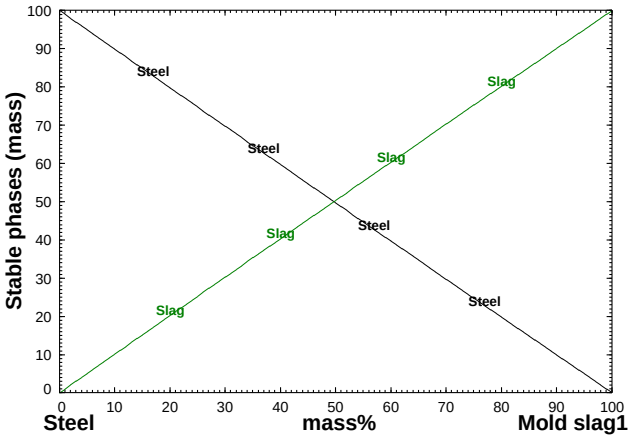

(a)

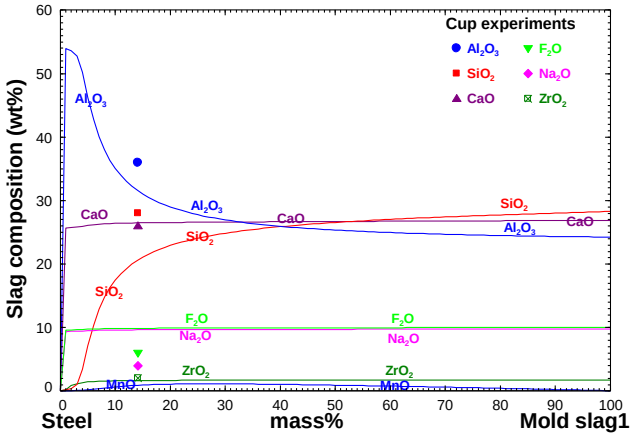

(b)

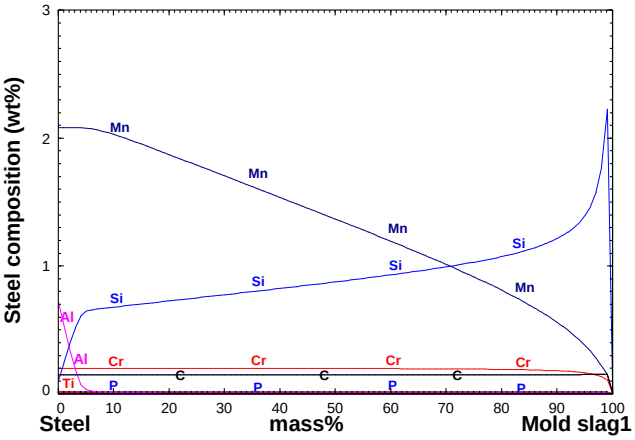

(c)

Figure 10. Reaction between the steel and mold slag (R3) calculated at 1570 °C under 1 bar total pressure, (a) the reaction products, (b) the 'mold slag3' composition (symbols represent the experimental mold slag composition) and (c) the 'steel3' composition

mold slag, respectively. As seen, other components of mold slag such as CaO, ZrO_2, Na_2O and F_2O remain constant. The mixing ratio of steel / mold slag was 6/1 in the experiment. Assuming the entire bulks of mold slag and steel reacted together and the reaction reached equilibrium, the composition of mold slag after the experiment was plotted as symbols against the calculations in Figure 10(b) at ~14 wt% mold slag. Al and Si amounts of steel were calculated to be 0.0077 and 0.6970 wt%, respectively, in comparison to experimentally measured values of 0.0021 and 0.9180 wt%, respectively. That is, in addition to the mold slag – steel exchange reaction, another reaction should have contributed to the further decrease in steel Al content. This could be the Al oxidation by dissolved O from the CO(g) reaction with steel. CO(g) generated from the refractory carbothermic reaction (R1) dissolves in steel as C and O, CO(g) = [C] + [O], and O oxidizes Al to form Al_2O_3, 2[Al] + 3[O] = (Al_2O_3). This was further proved by the Al_2O_3 rim formation at the CO bubble – steel interface around the elephant feet in the laboratory scale experiments as illustrated in Fig. 11.

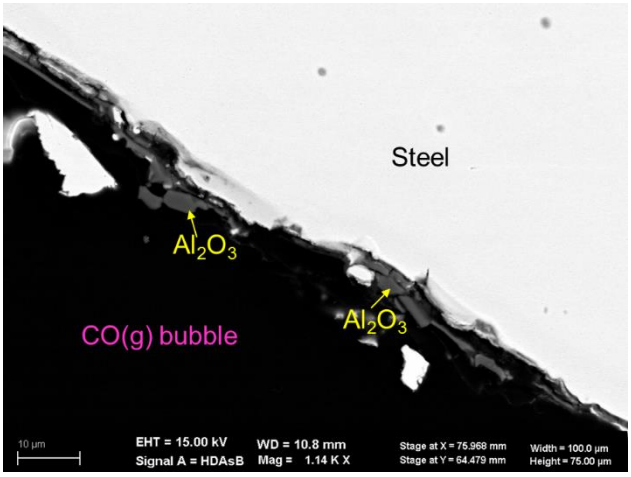

Figure 11. Formation of Al_2O_3 rim at the steel – CO bubble interface around the elephant feet in laboratory scale experiments

Conclusion

The submerged entry nozzle (SEN) – mold slag – steel interfacial reactions were modeled from the equilibrium thermodynamic point of view based on laboratory scale cup experiments and post-mortem SEN samples from plant. This approach was a step forward in understanding the relation between interactions in and around the SEN and the extent of mold slag modification process and SEN life-time.
The refractory self-reaction, refractory – mold slag carbothermic reaction, the gas back-infiltration into the SEN and deposit formation across the SEN, and the steel – mold slag exchange reaction were calculated using the developed model.
The SEN self-reaction (partial melting and gas evolution) during heating, noticeable decarburization in reaction with the mold slag and internal chemical reactions with the gas phase under the influence of an existing underpressure all endanger the SEN integrity and performance. On the other hand, the mold slag experiences a chemical modification process which may eventually impact its thermophysical properties and functionality. The mold slag not only picks up Al from steel but also can dissolve significant amounts of SEN refractory including Al_2O_3 (more than two times of its original weight). The extensively modified mold slag remains super liquid and can easily crawl around the SEN at the steel interface. Moreover, the aluminous mold slag does not crystallize cuspidine as the primary phase upon cooling.

Abbreviations

SEN	Submerged entry nozzle
EPMA	Electron probe micro analysis
XRF	X-ray fluorescence
BSE	Back-scattered electron
EDS	Energy dispersive spectroscopy
$C_2M_2A_{14}$	$Ca_2Mg_2Al_{28}O_{46}$
Cus	$Ca_4Si_2F_2O_7$ (cuspidine)
NC_3A_8	$Na_2Ca_3Al_{16}O_{28}$
CM'_2	$CaMn_2O_3$
CM_2A_8	$CaMg_2Al_{16}O_{27}$
Mel	Melilite
CaFl	Low-temperature CaF_2
ZrO_m	Monoclinic ZrO_2
ZrO_t	Tetragonal ZrO_2
Neph	Nepheline
FeldA	Feldspar

References

[1] Hibbeler, L.; Lui, R.; Thomas, B.G.: Review of mold flux entrainment mechanisms and model investigation of entrainment by shear layer instability; Proc. 7th ECCC, Düsseldorf (2011).
[2] Mukai, K.; Toguri, J. M.; Stubina, N. M.; Yoshitomi, J.: A mechanism for the local corrosion of immersion nozzles; ISIJ Int., 29 (1989), P. 469 -76.
[3] Sasai, K.; Mizukam, Y.; Reaction and mechanism between low carbon steel alumina graphite immersion nozzle; ISIJ Int., 34 (1994), P. 802-9.
[4] Dick, A. F.; Yu, X.; Pomfret, R. J.; Coley, K.S.: Attack of submerged entry nozzles by mould flux and dissolution of refractory oxides in the flux; ISIJ Int., 37 (1997), P. 102-8.
[5] Harmuth, H.; Xia, Guangmin: Interaction steel/slag/submerged entry nozzle and its impact on refractory wear – thermochemical process simulation; ISIJ Int., 55 (2015), P. 775-80.
[6] Zinngrebe, E.; Wijngaarden, M.; Mensonides, F.; Kalter, R.; Laan, S.; Rijnders, M.; Moosavi-Khoonsari, E.: Microstructures of mould slag crawling at the SEN during thin slab casting; METEC & 4th ESTAD (European Steel Technology and European Days), Düsseldorf, Germany, 24 - 28 June (2019).
[7] www. FactSage.com
[8] Pelton, A. D.: Phase diagrams and thermodynamic modeling of solutions; Elsevier, 5th

ed., edited by Laughlin D. E. and Hono K. (2019), P. 136-7.
[9] Iyi, N.; Göbbels, M.; Matsui, Y.: The Al-rich part of the system CaO-Al_2O_3-MgO Part II. Structure refinement of two new magnetoplumbite-related phases; J. Solid State Chem., 120 (1995), P. 364-71.